DOI: 10.1002/cmdc.200800104

Thiobarbiturates as Sirtuin Inhibitors: Virtual Screening, Free-Energy Calculations, and Biological Testing

Urszula Uciechowska,[a] Jörg Schemies,[b] Robert C. Neugebauer,[b] Elisabeth-Maria Huda,[b] Martin L. Schmitt,[b] Rene Meier,[a] Eric Verdin,[c] Manfred Jung,[b] and Wolfgang Sippl*[a]

NAD^+-dependent histone deacetylases (sirtuins) are enzymes that cleave acetyl groups from lysine residues in histones and other proteins. Potent selective sirtuin inhibitors are interesting tools for the investigation of the biological functions of these enzymes and may be future drugs for the treatment of cancer or neurodegenerative diseases. Herein we present the results from a protein-based virtual screen of a commercial database with subsequent biological testing of the most promising compounds. The combination of docking and in vitro experimental testing resulted in the identification of novel sirtuin inhibitors with thiobarbiturate structure. To rationalize the experimental results, free-energy calculations were carried out by molecular mechanics Poisson–Boltzmann/surface area (MM-PBSA) calculations. A significant correlation between calculated binding free energies and measured Sirt2 inhibitory activities was observed. The analyses suggested a molecular basis for the interaction of the identified thiobarbiturate derivatives with human Sirt2. Based on the docking and MM-PBSA calculations we synthesized and tested five further thiobarbiturates. The MM-PBSA method correctly predicted the activity of the novel thiobarbiturates. The identified compounds will be used to further explore the therapeutic potential of sirtuin inhibitors.

Introduction

Histone deacetylases (HDACs) are transcriptional regulators that deacetylate histones and various nonhistone proteins. This enzymatic activity affects the conformational state and activities of the substrate proteins.[1] Four classes of histone deacetylases have been described in humans: Classes I, II, and IV are zinc-dependent amidohydrolases, and 11 subtypes have been described (HDAC1–HDAC11). Class III enzymes rely on NAD^+ for catalysis, with subsequent formation of nicotinamide and *O*-acetyl-ADP-ribose as a result of transacetylation. Based on their homology to the yeast histone deacetylase Sir2p, the NAD^+-dependent HDACs are known as sirtuins, and seven members (Sirt1–Sirt7) have been identified in humans.[2]

Although class I, II, and IV HDACs have been identified as valid anticancer targets, and an initial inhibitor (Vorinostat) has been approved for clinical use,[3] much less is known about the consequences of class III HDAC inhibition.[2] Sirtuins have been linked to aging, and overexpression of sirtuins leads to a prolonged lifespan in yeast.[4] Sirtuin activity has been recently tied to the pathogenesis of HIV[5] and cancer,[6–8] as well as neurological diseases.[9] Only a limited number of sirtuin inhibitors are known, and some do not inhibit human subtypes.[10,11] The first synthetic inhibitor that was discovered is sirtinol (**1**)[12] (Figure 1), but in certain cases it has been shown that precipitation of the enzyme by the inhibitor contributes to the in vitro inhibition.[13] Structure–activity relationships (SAR) of sirtinol analogues were reported recently.[14] β-Arylsplitomicin derivatives **2**, which were recently discovered by us, were found to be potent inhibitors ($IC_{50} \sim 1$ μM) of human isoforms.[5] Further Sirt2 inhibitors have been discovered through a virtual screening approach, but cellular activity and verification of protein hyperacetylation have not been demonstrated.[15–17] The sirtuin inhibitor cambinol (**3**) was discovered from random screening, and for the first time anticancer activity in an animal model could be demonstrated with this compound.[18] Lately, indoles such as **4**, with activity down to ~0.1 μM have been presented.[19] Similar potencies have been observed in analogues of suramin,[20] which had been previously shown to be a sirtuin inhibitor.[21] Using a focused library screening approach, we had identified kinase inhibitors such as Ro-318220 (**5**) as new lead structures for sirtuin inhibitors that target the adenosine binding pocket.[22]

Recently, we carried out SAR studies on β-arylsplitomicin derivatives.[23] Selected compounds were tested for antiproliferative activity and for intracellular tubulin acetylation. Furthermore, we were able to show by new derivative **6** that a

[a] *U. Uciechowska,[+] R. Meier, Prof. Dr. W. Sippl*
Martin-Luther Universität Halle-Wittenberg
Department of Pharmaceutical Chemistry
Wolfgang-Langenbeckstr. 4, 06120 Halle/Saale (Germany)
Fax: (+49) 345-5527355
E-mail: wolfgang.sippl@pharmazie.uni-halle.de

[b] *J. Schemies,[+] Dr. R. C. Neugebauer, E.-M. Huda, M. L. Schmitt, Prof. Dr. M. Jung*
Albert Ludwigs-Universität Freiburg
Institute of Pharmaceutical Sciences
Albertstr. 25, 79104 Freiburg (Germany)

[c] *Prof. Dr. E. Verdin*
University of California
Gladstone Institute of Virology and Immunology
1650 Owens Street, San Francisco, CA 94158 (USA)

[+] *These authors contributed equally to this work.*

Supporting information for this article is available on the WWW under http://dx.doi.org/10.1002/cmdc.200800104.

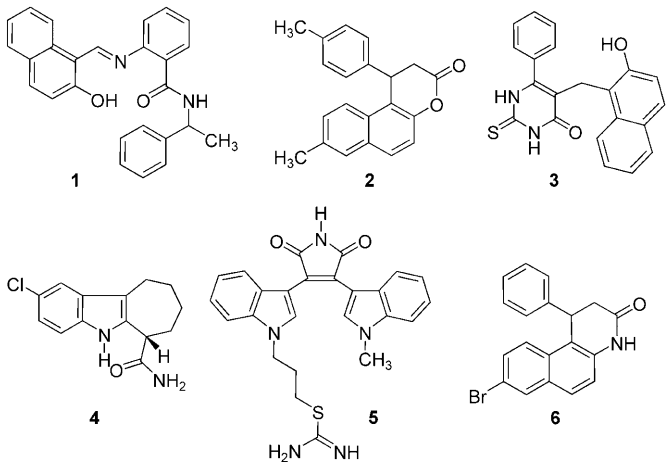

Figure 1. Known sirtuin inhibitors.

replacement of the lactone ring in splitomicins by a lactam substructure is well tolerated, provided that other features that increased the potency of splitomicin are retained. Because the lactam ring, unlike the lactone ring in splitomicin, is not expected to hydrolyze, this result suggested that splitomicins may act as reversible inhibitors at least for human subtypes and not as acylating agents, as had been suggested for yeast enzymes.[24]

The purpose of this study was to find new substances that will inhibit human sirtuins. We used a synergistic approach that combines the benefits of structure-based virtual screening and experimental testing with validated sirtuin inhibition assays to subsequently screen only a limited number of the top-ranking compounds. Because several 3D structures of sirtuin proteins are known, it was possible to apply target-based virtual screening technologies to search for novel sirtuin inhibitors. We decided to perform a multi-step virtual screening experiment starting with a prefiltered compound library containing over 328 000 unique molecules and a combination of similarity-based screening and ligand docking. The virtual screen was followed by free-energy calculations applying the MM-PBSA[25] approach to get a better estimate of the ligand binding free energy. The applied approach yielded not only an enriched subset of compounds for subsequent analysis but also uncovered promising lead candidates that represent valuable tools to further explore the therapeutic potential of sirtuin inhibitors.

Results and Discussion

Analysis of the Sirt2 binding site

The X-ray structures of several Sir2 proteins have been published over the last few years, whereas no 3D structure is available for Sirt1.[26,27] The structure of the catalytic domain of Sir2 consists of a large classical Rossmann fold and a small zinc binding domain. The interface between the large and the small subdomain is commonly subdivided into A, B, and C pockets. This division is based on the interaction of adenine (A), ribose (B), and nicotinamide (C), which are parts of the NAD^+ cofactor. Whereas the interaction of adenine and ribose is similar in all available sirtuin X-ray structures, multiple binding modes have been observed for the nicotinamide portion. Several so-called productive and nonproductive conformations of NAD^+ have been observed in the crystal structures from Archaea, reflecting the flexibility of the cofactor and the corresponding binding site. Whereas the human Sirt2 crystal structure contains no bound ligands, the X-ray structure of a Sir2 homologue from Archaea[26] shows that the peptide substrate binds in a cleft between the large and small domains. The acetyllysine residue inserts into a conserved hydrophobic pocket, and NAD^+ binds nearby. In the case of the human Sirt2 X-ray structure,[27] which was crystallized as a trimer, no structural information about NAD^+ or inhibitor binding is available. However, owing to the homology with bacterial sirtuins, it is clear that the interaction between NAD^+ and Sirt2 is similar to that observed in the bacterial X-ray structure complexes.

We previously described the development of other series of Sirt2 inhibitors, including adenosine mimetics such as the bisindolylmaleimide **5**,[22] suramin derivatives, and β-arylsplitomicin derivatives[20] (e.g. compound **2**). Based on docking studies that we carried out for human Sirt2 and competition experiments with NAD^+, we found that the compounds interact with the adenine (for **5**) and the nicotinamide subpocket (for **2** and **6**), respectively. The analysis of the X-ray structure of human Sirt2 (which contains three monomers) and preliminary docking simulations using the known inhibitors **2**, **3**, **4**, and **6** showed that the compounds interact with the nicotinamide subpocket (C) of Sirt2. The consideration of four water molecules within the binding site that are observed in the three Sirt2 monomers of the structure deposited under PDB code 1J8F significantly improved the docking results. β-Phenylsplitomicin **2** makes a hydrogen bond to the water molecule bonded to Gln167. The β-phenyl substituent fits into a hydrophobic channel and is sandwiched between Phe119 and His187. This channel represents the binding site for the acetylated lysine residue of the substrate. The docking of cambinol (**3**) and the lactam **6** showed that the NH group of the inhibitors interact with Gln167 located in the nicotinamide binding pocket C (Phe96, Gln167, Asn168, Ile169, His187) whereas the carbonyl group of **3** accepts a hydrogen bond from His187 (Figure 2).

Based on the docking results of the previously reported splitomicin derivatives, we prepared a variety of novel compounds (**13**–**16**) with substituents at the 3- and 4-positions of the β-phenyl group. The docking results showed that the phenyl ring is located at the entrance of the acetyllysine substrate channel. Therefore, we suggested that the addition of a hydrophobic substituent at the 4-position of the β-phenylsplitomicins would increase the inhibitory potency. The subsequent synthesis (Scheme 1 and Scheme 2) and biological testing of compounds **13**–**16** showed that the presence of an ethyl group at the 4-position results in the most potent inhibitor of this series (Table 1). Bulkier hydrophobic groups at the 4-position or polar groups at the 3-position resulted in a decrease in the inhibitory activity.

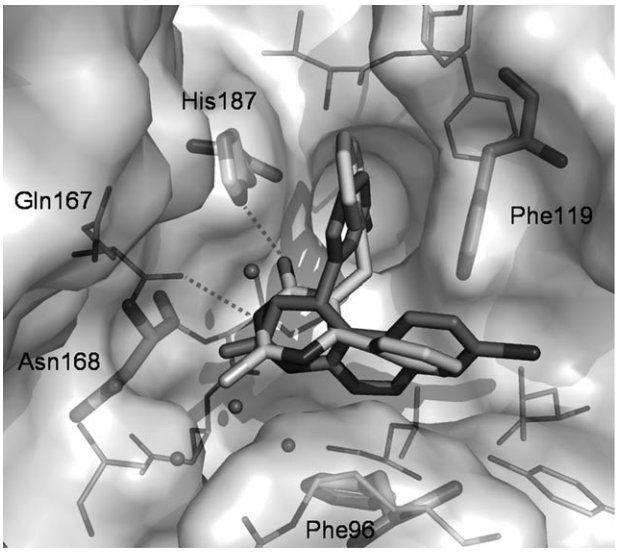

Figure 2. Comparison of the docking results obtained for **3** (white) and **6** (gray) at Sirt2. The four water molecules used in the docking study are displayed as balls. Hydrogen bonds are indicated by the dashed lines. The Connolly molecular surface of the binding pocket is displayed.

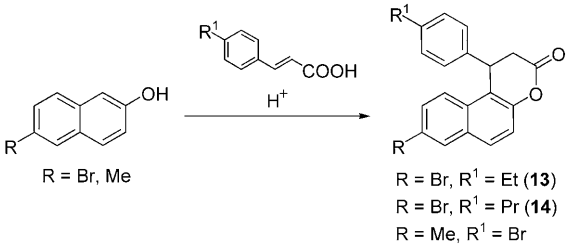

Scheme 1. Cyclization of naphthols via Friedel–Crafts alkylation.

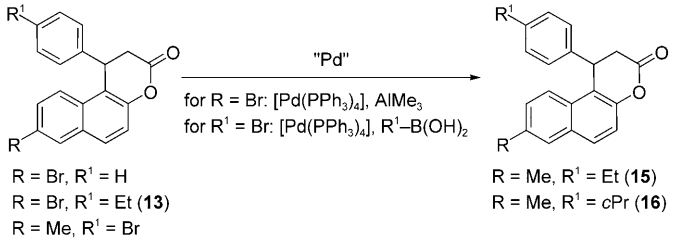

Scheme 2. Pd-catalyzed reactions on splitomicin derivatives.

Visual analysis of the GRID interaction fields further supports the binding mode obtained by GOLD[28] docking. The most favorable interaction with the hydrophobic methyl probe was observed in the acetyllysine channel and the proximal amino acid residues Phe119, Val233, and Phe234. The favored interaction with hydrogen bond acceptors (calculated with the GRID carbonyl probe) was observed near the polar residues Gln167 and Asn168 and is in agreement with the location of the thiobarbiturate oxygen atom (see figure 1 in the Supporting Information).

Virtual screening

The virtual screen was carried out with the Chembridge database (Chembridge Corporation, San Diego, CA, USA) containing a library of ~328 000 compounds. The database was filtered as described below in the Experimental Section. To decrease the number of molecules to be docked we applied simple similarity-based filtering using MACCS keys. A total of 390 compounds similar to **3** were selected and docked into the binding pocket of Sirt2; 131 molecules were successfully docked into the nicotinamide binding pocket (showing a GoldScore between 62 and 30). The final selection of a small subset of compounds was based on visual inspection of the binding mode (only molecules showing a hydrogen bond to Gln167 were considered) and on the lipophilicity of the compounds (lower log*P* values favored). Five barbiturate and thiobarbiturate derivatives were selected, which were found between rank 1 and 61 (Figure 3). The five compounds were purchased from Chembridge and tested in an in vitro assay[29] for their ability to inhibit human Sirt2 (Table 2).

The interaction of the most potent compound **9** with human Sirt2 is shown as an example in Figure 4A and 4B. A common feature of the active inhibitors is the interaction (hydrogen bond) of one barbiturate/thiobarbiturate NH group with the backbone carbonyl group of Gln167 and the hydrogen bond between the barbiturate CO group and His187. The

Table 1. Energy contributions to the free energy of binding of the splitomicin derivatives as obtained by the MM-PBSA approach.[a]

Compd	ΔE_{el}	ΔE_{vdW}	ΔE_{GBSA}	ΔH_{tot}	$T\Delta S_{tot}$	ΔG_{calcd}	Sirt2 $IC_{50} \pm SE$ [μM]	ΔG_{exptl}
2	−2.09	−38.68	7.23	−33.54	−25.79	−7.64	1.5 ± 0.3	−7.94
6	−2.87	−34.10	12.24	−24.73	−17.08	−7.65	6.4 ± 0.3	−7.08
12	−7.81	−30.87	11.26	−27.42	−21.50	−5.92	10.6 ± 1.0	−6.78
13	−2.31	−32.00	8.13	−26.18	−17.72	−8.46	1.2 ± 0.4	−8.07
14	1.27	−32.67	6.01	−25.38	−20.86	−4.52	4.8 ± 2.3	−7.25
15	−8.27	−39.05	16.29	−31.03	−18.00	−13.30	2.8 ± 1.8	−7.57
16	−3.50	−32.56	15.8	−20.26	−15.60	−4.66	5.4 ± 0.2	−7.18
17	−5.00	−28.60	11.49	−22.12	−18.72	−3.40	19.5 ± 9.7	−6.42
18	−0.14	−42.21	17.45	−24.90	−21.22	−3.68	19.7 ± 5.5	−6.41
19	−2.00	−35.81	13.76	−24.06	−14.01	−10.05	2.3 ± 0.3	−7.69
20	−3.81	−37.77	18.41	−23.18	−17.03	−6.15	3.4 ± 0.3	−7.45
21	−3.80	−35.25	12.53	−26.52	−17.47	−9.05	4.4 ± 0.6	−7.30
22	−4.65	−34.28	14.23	−24.70	−11.90	−12.80	3.1 ± 0.5	−7.51
23	−11.10	−34.57	22.80	−22.88	−20.26	−2.62	20.0 ± 8.0	−6.41
24	2.24	−31.94	4.19	−25.51	−15.55	−9.96	5.2 ± 1.0	−7.20

[a] ΔE_{el} and ΔE_{vdW} are respectively the electrostatic and van der Waals energies of binding in the gas phase; ΔE_{GBSA}: contributions to the solvation free energy; ΔH_{tot} is the enthalpy of binding, $T\Delta S_{tot}$ is the entropy of binding, and ΔG_{calcd} is the calculated binding free energy. Biological data are determined as described in the Experimental Section, or are taken from reference [35]. ΔG_{exptl} values were calculated by $\Delta G_{exptl} = -RT \ln(IC_{50})$.

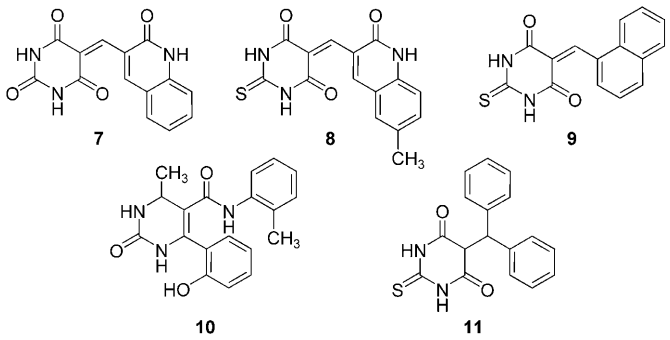

Figure 3. Molecular structures of the five hits from the virtual screen of the Chembridge database.

Table 2. Inhibition of Sirt1 and Sirt2 by the hits derived from the virtual screen.

Compd	Sirt1 $IC_{50} \pm SE$ [μM]	Sirt2 $IC_{50} \pm SE$ [μM]
7	34.2%[a]	61 ± 3.5
8	12.9 ± 2.8	11.3 ± 1.7
9	13.2 ± 2.5	9.1 ± 5.8
10	NA[b]	130.7 ± 47.2
11	47.9 ± 2.8	40.7 ± 3.9

[a] Percent inhibition at 50 μM. [b] Inhibition < 10% at 50 μM.

bulky naphthyl or hydroxyquinoline substituent is directed into the acetyllysine substrate channel and undergoes van der Waals interactions with the aromatic ring system of Phe119 and His187. The binding mode of the novel thiobarbiturate inhibitors is similar to that observed for cambinol (**3**) (Figure 2).

Compounds **7** and **8** can be present in two tautomeric forms. In the Chembridge database both molecules are stored as the hydroxyquinoline tautomer, which was also considered for the virtual screening study. We also generated the pyridone tautomer and docked it into the Sirt2 binding pocket. A similar binding mode was observed for the pyridone tautomer, placing the pyridone ring between the aromatic side chains of Phe119 and His187 (RMSD: 0.2 Å). Semi-empirical quantum mechanical calculations using the AM1 method were carried out to calculate the potential energies of the two tautomers of **7** and **8**. Such calculations carried out in vacuo yielded an energetic preference for the pyridone tautomer, whereas the GoldScores were observed to be higher for the hydroxyquinoline tautomer. Similar results were derived with X-Score, ChemScore, and ASP Score.[28] Based on the calculated docking pose and scores, no final decision can be made as to which tautomer is more likely to interact with the Sirt2 active site.

Using the calculated GoldScore values, we observed no correlation between the scores and the determined IC_{50} values. The poor correlation between docking scores and biological data is a major problem with current docking approaches.[30] Therefore, we focused on a more sophisticated method for the analysis of key interactions necessary for high inhibitory activity.

MM-PBSA approach

The virtual screen resulted in five barbiturates and thiobarbiturates including the active inhibitors **8** and **9**. As we did not observe any correlation between the docking scores and pIC_{50} values, we calculated the binding free energy by using the MM-PBSA approach. To increase the number of compounds used to establish a quantitative model we added the developed β-arylsplitomicin inhibitors reported in Table 1.[23]

The Sirt2–inhibitor complexes derived from the docking study were used as starting complexes for molecular dynamics (MD) simulations using the AMBER program. These simulations

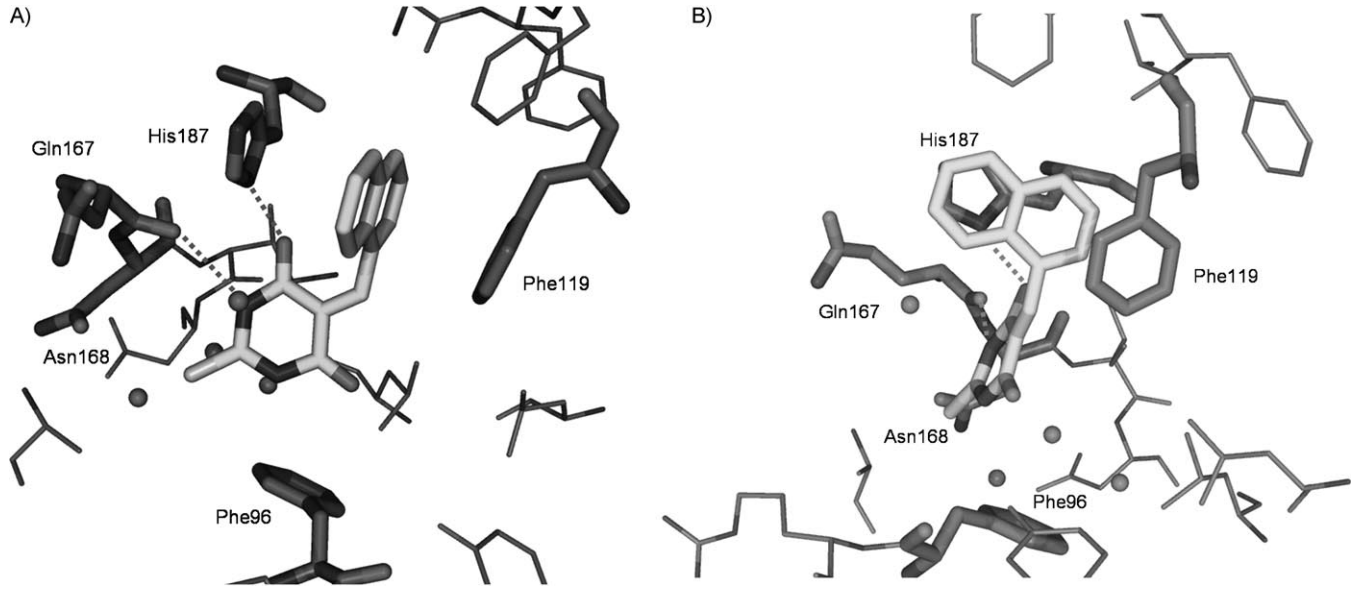

Figure 4. A) Predicted binding mode of **9** at the nicotinamide binding site of human Sirt2. The four water molecules used in the docking study are displayed as balls. Hydrogen bonds are indicated by the dashed lines. B) View rotated by 90°.

showed that the generated complexes are stable during the 5-ns free MD simulation (see figure 2 in the Supporting Information). The inhibitor interactions observed in the starting structures (obtained by GOLD) were generally maintained during the MD simulations. In our analysis of the RMSD of the complex structures (heavy atoms), we found that the maximum deviations are < 2 Å.

The MD trajectories were further analyzed by successively applying the MM-PBSA method.[31–35] In this approach, the absolute free energy of a system is estimated from a combination of molecular mechanics, i.e. Poisson–Boltzmann estimation of the electrostatic free energy, an estimation of the solvation free energy determined from the exposed surface area, and an estimate of the entropy of the system derived from normal mode calculations.

To establish a more quantitative SAR, we used a ligand data set containing the five thiobarbiturates and barbiturates from the virtual screen and 15 splitomicin derivatives that were recently developed and tested in our laboratory (Figure 5).[23] The synthesis of the new splitomicins (**13**–**16**) follows the principles outlined in our previous report on that compound class (Schemes 1 and 2).[23] All compounds were tested in the same biological assay. In the case of the splitomicin derivatives, the assays were carried out with the racemic mixtures. However, we recently showed that by separating the *R* and *S* stereoisomers of **2** that the *R* isomer is the active component (IC_{50} (*R*)-**2**: 1.0 μM, IC_{50} (*S*)-**2**: > 100 μM, IC_{50} (±)-**2**: 1.5 μM).[23] Therefore, the *R* isomers of the splitomicin derivatives were used for the docking and free-energy calculations, whereas the biological data were determined with the racemic mixtures. Because the splitomicin derivatives are structurally very similar, it can be suggested that for all compounds, the *R* isomer represents the active component for biological activity.

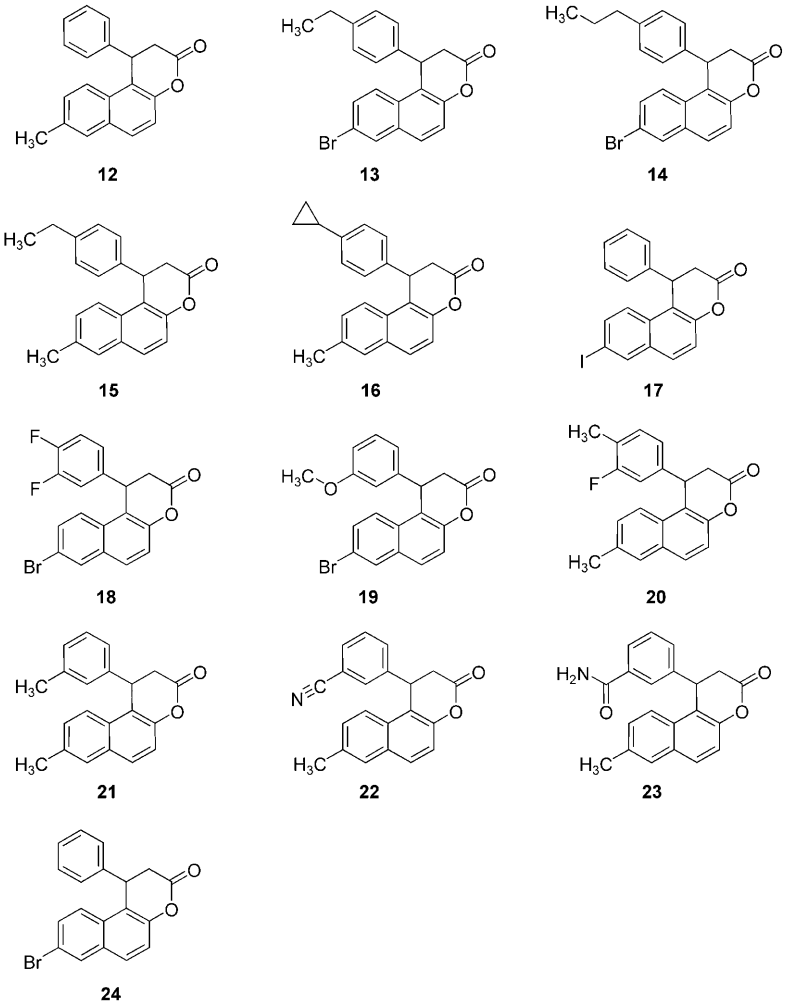

Figure 5. Molecular structures of the 15 splitomicin compounds used for the MM-PBSA calculation.

The binding free energies for the barbiturates and the splitomicin derivatives were estimated using the MM-PBSA method as described in the Experimental Section below (Table 1 and Table 3). The calculated binding free energies ΔG_{calcd} for the two novel thiobarbiturate inhibitors are -4.24 kcal mol^{-1} (for **8**) and -2.98 kcal mol^{-1} (for **9**). As shown in Tables 1 and 3, the compounds form van der Waals/hydrophobic interactions, while intermolecular electrostatic interactions also contribute to the binding affinity. The barbiturates show lower binding free energies than the splitomicin derivatives. On the other hand, the electrostatic contribution to the solvation free energy of the active thiobarbiturates is more favorable.

To determine whether MM-PBSA is useful for further lead optimization, the correlation between calculated values (binding free energies ΔG_{calcd} and binding enthalpies ΔH_{tot}) and the experimental IC_{50} values of the ligands was analyzed. It is clear that this approach represents only a rough approximation, as biological data from an in vitro assay are used instead of pure thermodynamic values from calorimetric studies. Therefore an

Table 3. Energy contributions to the free energy of binding of the thiobarbiturate and barbiturate derivatives as obtained by the MM-PBSA approach.[a]

Compd	ΔE_{el}	ΔE_{vdW}	ΔE_{GBSA}	ΔH_{tot}	$T\Delta S_{tot}$	ΔG_{calcd}	ΔG_{exptl}
7	−5.59	−28.71	21.32	−12.97	−17.28	4.31	−5.75
8	−7.38	−32.20	19.61	−19.96	−16.98	−2.98	−6.74
9	−19.10	−31.79	30.35	−20.54	−16.30	−4.24	−6.87
10	−7.89	−31.20	24.3	−14.79	−15.56	0.77	−5.29
11	−13.90	−28.23	25.31	−16.82	−14.54	−2.28	−5.98

[a] ΔE_{el} and ΔE_{vdW} are respectively the electrostatic and van der Waals energies of binding in the gas phase; ΔE_{GBSA}: contributions to the solvation free energy; ΔH_{tot} is the enthalpy of binding, $T\Delta S_{tot}$ is the entropy of binding, and ΔG_{calcd} is the calculated binding free energy. ΔG_{exptl} values were calculated by $\Delta G_{exptl} = -RT \ln(IC_{50})$.

ideal correlation is not expected. However, we recently showed that the MM-PBSA approach is useful to discriminate between weak and strong sirtuin inhibitors.[23]

To calculate ΔG_{calcd}, the AMBER module Nmode was used (see Experimental Section below for details) to estimate the entropic contribution. As shown in Figure 6, where the experimental activities are plotted versus the calculated binding free energies, there is a significant correlation between the binding free energy ΔG ($r = 0.83$, $r^2 = 0.69$, SD = 0.40) and the biological activity. For the enthalpy ΔH_{tot} the correlation is lower ($r = 0.69$, $r^2 = 0.47$, SD = 0.52) due to one outlier: compound **12**. Removing the outlier resulted in a model with a regression coefficient of $r^2 = 0.65$ for the enthalpy model. To test the predictive ability of the model, we carried out leave-one-out (LOO) cross validation. For the binding free energy ΔG model we obtained a cross-validated q^2_{LOO} value of 0.61 (Supporting Information).

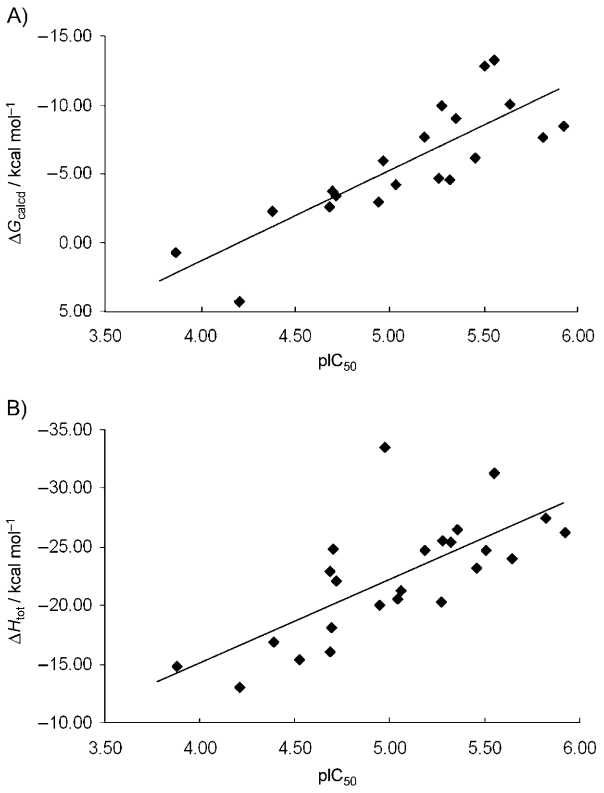

Figure 6. A) Correlation between calculated MM-PBSA binding free energies ΔG_{calcd} and the Sirt2 pIC_{50} values. B) Correlation between calculated MM-PBSA binding enthalpies ΔH_{tot} and the Sirt2 pIC_{50} values.

In contrast to the applied GOLD docking, the MM-PBSA approach does take protein flexibility into account. This is a significant contribution to improved ligand scoring. Another reason for the improved results with the MM-PBSA calculations is that the force field used in combination with continuum solvent electrostatics to calculate ΔG_{solv} provides a more accurate description of the ligand binding than the empirical GOLD scoring function. In contrast to more rigorous methods such as free-energy perturbation (FEP) or thermodynamic integration (TI), MM-PBSA is faster by several orders of magnitude. However, the approximations inherent to MM-PBSA result in larger errors than those associated with more sophisticated methods such as FEP or TI. In particular, estimation of the entropic term on the basis of the trajectories is often connected with a large standard deviation. This can also be recognized when considering the significant deviations of $T\Delta S_{tot}$ for structurally similar compounds (Tables 1 and 3). To overcome the entropy problem, it was suggested to increase the simulation time and to use smaller snapshot sizes for sampling the entropic term. However, for larger data sets this dramatically increases the time required for the MD simulations. Therefore, finding an acceptable balance between accuracy and simulation time is still a challenge.

Synthesis of modified thiobarbiturates

The analysis of the MD simulation showed that the most active thiobarbiturates, compounds **8** and **9**, form stable complexes with Sirt2 (RMSD values < 1 Å, see figure 1 in the Supporting Information). The thiobarbiturate ring of **8** and **9** makes hydrogen bonds with His187 and the backbone NH group of Gln167. The hydrogen bond between His187 and the thiobarbiturate moiety of **8** and **9** was found to be stable during the 5-ns simulation (see figure 3 in the Supporting Information), whereas the direct hydrogen bond to the backbone NH group of Gln167 was observed only at the beginning of the simulation. However, we observed several water-mediated hydrogen bonds between the thiobarbiturates and the polar residues of the pocket (not shown).

The analysis of the GRID interaction field derived with the hydrophobic methyl probe showed a favorable interaction field above the naphthyl substituent of docked compound **9** (figure 1 in the Supporting Information). Therefore, we designed and synthesized five thiobarbiturates (**25**–**29**) with modified hydrophobic substituents (Figure 7 and Scheme 3). A similar docking pose as calculated for **8** and **9** were obtained for the novel thiobarbiturates. As an example, the interaction of the most potent thiobarbiturate **25** with the Sirt2 binding

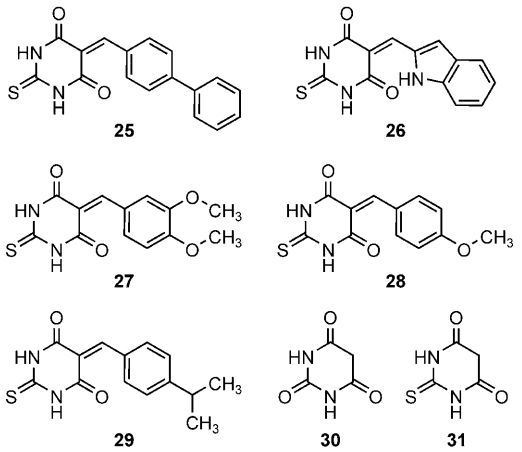

Figure 7. Molecular structures of barbituric acid, thiobarbituric acid, and five novel thiobarbiturates.

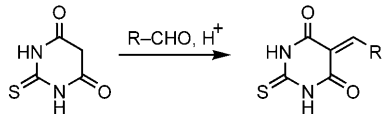

Scheme 3. Synthesis of arylidene thiobarbiturates.

pocket is shown in Figure 8. The calculated ΔG values of the five compounds were found to be < -4.2 kcal mol^{-1}, indicating that they should be just as, or more potent than, the thiobarbiturate **9** (Table 4 and Table 5). Subsequent biological testing showed that all five new thiobarbiturates are active against Sirt2 at concentrations < 30 μM. In general, good agreement between ΔG_{calcd} and pIC_{50} values for the five novel thiobarbiturates were obtained (Figure 9). Compound **25**, bearing a biphenyl group, is the most active thiobarbiturate toward Sirt2, in agreement with the predicted MM-PBSA ΔG_{calcd} value (Table 5). The biphenyl group fits in the acetyllysine substrate channel and interacts with the surrounding aromatic side chains (Figure 8). To further support our hypothesis that the hydrophobic aryl group is important for sirtuin activity, we experimentally tested unsubstituted barbituric and thiobarbituric acid. Neither compound showed inhibition of Sirt2 at a concentration of 50 μM.

Table 4. Inhibition of Sirt1 and Sirt2 by the novel synthesized thiobarbiturates.

Compd	Sirt1 $IC_{50} \pm SE$ [μM]	Sirt2 $IC_{50} \pm SE$ [μM]
25	50.5 ± 9.1	8.7 ± 0.7
26	5.9 ± 0.3	20.3 ± 1.5
27	23.3 %[a]	30.1 ± 3.1
28	61.6 ± 5.3	20.0 ± 1.7
29	12.4 ± 0.5	14.7 ± 2.1
30	NA[b]	NA[b]
31	NA[b]	NA[b]

[a] Percent inhibition at 50 μM. [b] Inhibition < 10% at 50 μM.

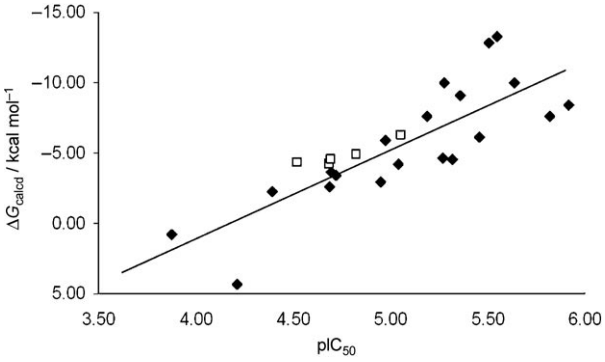

Figure 9. Correlation between calculated MM-PBSA binding free energies ΔG_{calcd} and the Sirt2 pIC_{50} values of the training set (◆) and test set compounds (□).

Enzyme inhibition

All compounds were tested in initial studies for Sirt2 inhibition at concentrations of 50 and 100 μM in a homogeneous deacetylase assay using a fluorescent acetyllysine derivative[13] that was previously developed by our research group.[29] Usually, IC_{50} value determinations performed only if > 50% inhibition at 50 μM is observed (see Tables 1 and 2). In the thiobarbiturate series we found compounds with potency down to the single-digit micromolar concentration range. For the most part, slight Sirt2 selectivity (up to sixfold in **25**) is found, whereas several compounds are unselective, and interestingly, the indole **26** is selective for Sirt1. Compound **25** is the most potent inhibitor of Sirt2, and **26** is the most potent against Sirt1. Experimental testing of the unsubstituted derivatives,

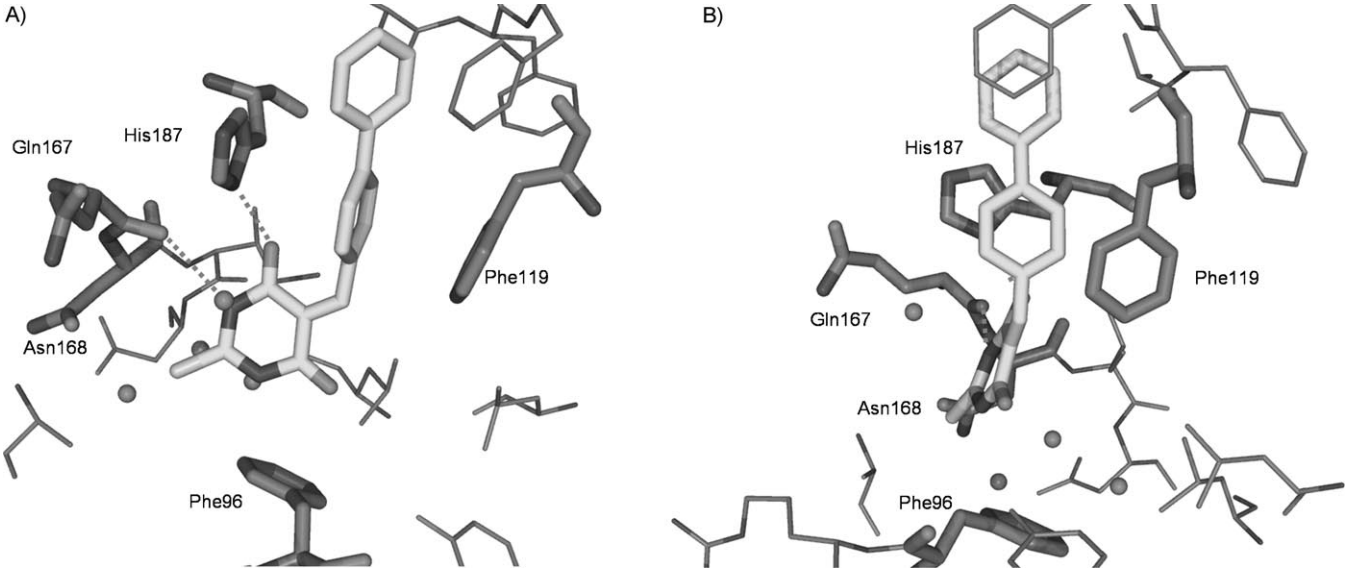

Figure 8. A) Predicted binding mode of **25** at the nicotinamide binding site of human Sirt2. The four water molecules used in the docking study are displayed as balls. Hydrogen bonds are indicated by the dashed line. B) View rotated by 90°.

Table 5. Energy contributions to the free energy of binding of the synthesized thiobarbiturates as obtained by the MM-PBSA approach.[a]

Compd	ΔE_{el}	ΔE_{vdW}	ΔE_{GBSA}	ΔH_{tot}	$T\Delta S_{tot}$	ΔG_{calcd}	ΔG_{exptl}
25	−5.16	−31.44	15.47	−21.13	−15.01	−6.29	−6.90
26	−8.53	−21.73	14.21	−16.05	−11.85	−4.20	−6.40
27	−5.76	−24.04	14.48	−15.32	−11.07	−4.31	−6.16
28	−7.54	−31.24	20.68	−18.10	−13.56	−4.54	−6.41
29	−3.14	−34.98	13.86	−24.26	−19.35	−4.91	6.59

[a] ΔE_{el} and ΔE_{vdW} are respectively the electrostatic and van der Waals energies of binding in the gas phase; ΔE_{GBSA}: contributions to the solvation free energy; ΔH_{tot} is the enthalpy of binding, $T\Delta S_{tot}$ is the entropy of binding, and ΔG_{calcd} is the calculated binding free energy. ΔG_{exptl} values were calculated by $\Delta G_{exptl} = -RT \ln(IC_{50})$.

barbituric acid **30** and thiobarbituric acid **31**, yielded no Sirt2 activity. In general, we tested all thiobarbiturates against both Sirt1 and Sirt2. Various activities have been reported toward Sirt1 and Sirt2 isotypes. For example, the anticancer activity of the unselective sirtuin inhibitor cambinol (**3**) in an animal model has been mechanistically linked mainly to substrates of Sirt1,[18] and it is unknown whether the Sirt2 inhibition contributes to its anticancer activity. Sirt1 and its activators seem to confer neuroprotection,[36] whereas a Sirt2 inhibitor was observed to be active in limiting neurotoxicity in a model of Parkinson's disease.[9] Therefore, sirtuin subtype selectivity is of great interest for the further design of potential drug candidates and the assessment of their potential side effects.

Conclusions

We have shown that a combination of target-based virtual screening and experimental in vitro testing can be used to discover novel sirtuin inhibitors. Polar interactions that anchor the identified thiobarbiturates into the binding site were found, and the placement of inhibitor-borne hydrophobic groups into the acetyllysine substrate pocket explains the need for this ligand hydrophobicity. In contrast, barbituric and thiobarbituric acid, which do not possess a hydrophobic group, were found to be inactive. Accurate relative binding free energies for a set of 20 Sirt inhibitors were calculated, paving the way for subsequent structural ligand modifications in search of more potent inhibitors. Based on the identified thiobarbiturate-based inhibitors, an initial series of derivatives with modified hydrophobic substituents was synthesized and biologically tested. MM-PBSA calculations were found to be useful as a second step after virtual screening in order to obtain more detailed and reliable information about the relative binding affinity than can be provided by simple docking and scoring programs. Further optimization of the identified thiobarbiturate-based sirtuin inhibitors can thus be performed in a more rational fashion.

Experimental Section

Chemistry

Materials and methods. Standard chemicals were purchased from Sigma–Aldrich or Lancaster. The syntheses for splitomicins were based primarily on protocols published previously by our research group.[23] Ethyl- and propylcinnamic acid were prepared from the corresponding benzaldehydes according to standard procedures. 6-Methyl-2-naphthol was synthesized as published.[23] ^{1}H NMR spectra were obtained on a Bruker Avance DRX 400 MHz spectrometer, and ^{1}H chemical shifts are reported in ppm (δ). Merck Kieselgel 60 was used for flash chromatography with mixtures of either cyclohexane and EtOAc or cyclohexane and CH_2Cl_2 as eluents so that the R_f value of the desired product was ~0.3.

General method: cyclization of naphthols with cinnamic acids using Amberlyst 15. The naphthol (3 mmol), the substituted cinnamic acid (6 mmol), and Amberlyst 15 ion-exchange resin (300 mg) were held at reflux in toluene (15 mL) overnight. The resin was filtered off and washed with toluene. The solvent was then removed under reduced pressure. Separation by column chromatography led to the isolation of the splitomicins.

1-(4-Bromophenyl)-8-methyl-1,2-dihydrobenzo[*f*]chromen-3-one. Preparation by the general method for cyclization starting from 6-methyl-2-naphthol (3 mmol), 4-bromocinnamic acid (6 mmol), and 300 mg Amberlyst 15 ion-exchange resin in toluene. Yield: 15% (white solid); ^{1}H NMR ($CDCl_3$): δ = 9.38 (d, 1H, ar, J = 8.8 Hz), 7.91 (d, 1H, ar, J = 9.0 Hz), 7.60 (m, 2H, ar, J = 8.4 Hz), 7.57 (s, 1H, ar), 7.52 (dd, 1H, ar, J = 8.8, 1.9 Hz), 7.42 (m, 2H, ar, J = 8.4 Hz), 7.16 (d, 1H, ar, J = 9.0 Hz), 5.37 (dd, 1H, C–H, J = 13.6, 3.1 Hz), 3.18 (dd, 1H, CH_2, J = 16.5, 13.6 Hz), 2.97 (dd, 1H, CH_2, J = 16.5, 3.1 Hz), 2.51 ppm (s, 3H, CH_3); ^{13}C NMR ($CDCl_3$): δ = 192.53 (C=O), 162.85 (ar, C–O), 137.64 (ar, C–C), 137.17 (ar, C–H), 134.60 (ar, C–C), 131.96 (2C, ar, 2×C–H), 131.81 (ar, C–H), 129.58 (ar, C–C), 129.28 (ar, C–C), 127.78 (2C, ar, 2×C–H), 127.61 (ar, C–H), 125.66 (ar, C–H), 122.68 (ar, C–C), 118.58 (ar, C–H), 112.57 (ar, C–C), 78.80 (C–H), 45.61 (CH_2), 21.16 ppm (CH_3); IR (ATR): $\tilde{\nu}$ = 1652, 1596, 1235, 1222, 1119, 1004, 823, 814 cm^{-1}; EIMS (*m/z*): 368 [^{81}Br*M*]$^+$, 366 [^{79}Br*M*]$^+$; [*M*]$^+$ ($C_{20}H_{15}BrO_2$): 367.24.

8-Bromo-1-(4-ethylphenyl)-1,2-dihydrobenzo[*f*]chromen-3-one (13). Preparation by the general method for cyclization starting from 6-bromo-2-naphthol (3 mmol), 4-ethylcinnamic acid (6 mmol), and Amberlyst 15 ion-exchange resin (300 mg) in toluene. Yield: 24% (white solid); ^{1}H NMR ($CDCl_3$): δ = 8.04 (d, 1H, ar, J = 2.0 Hz), 7.78 (d, 1H, ar, J = 9.0 Hz), 7.69 (d, 1H, ar, J = 9.0 Hz), 7.55 (dd, 1H, ar, J = 9.0, 2.0 Hz), 7.38 (d, 1H, ar, J = 9.0 Hz), 7.12 (m, 2H, ar), 7.03 (m, 2H, ar), 4.89 (dd, 1H, C–H, J = 2.4, 6.5 Hz), 3.22 (dd, 1H, C–H, J = 15.8, 6.5 Hz), 3.19 (dd, 1H, C–H, J = 15.8, 2.4 Hz), 2.60 (q, 2H, C–H, J = 7.7 Hz), 1.19 ppm (t, 3H, CH_3, J = 7.7 Hz); ^{13}C NMR ($CDCl_3$): δ = 166.8 (C=O), 149.9 (ar, C–O), 143.7 (ar, C–C), 137.4 (ar, C–C), 132.2 (ar, C–C), 130.7 (ar, C–H), 130.6 (ar, C–H), 129.6 (ar, C–C), 128.9 (ar, C–H), 128.7 (2C, ar, 2×C–H), 126.7 (2C, ar, 2×C–H), 124.9 (ar, C–H), 119.1 (ar, C–C), 118.7 (ar, C–H), 118.2 (ar, C–C), 37.4 (C–H), 37.3 (CH_2), 28.3 (CH_2), 15.3 ppm (CH_3); IR (ATR): $\tilde{\nu}_{max}$ = 1773, 1502, 1194, 1136, 892, 871, 815 cm^{-1}; EIMS: (*m/z*): 382 [^{81}Br*M*]$^+$, 380 [^{79}Br*M*]$^+$; [*M*]$^+$ ($C_{21}H_{17}BrO_2$): 381.27.

8-Bromo-1-(4-propylphenyl)-1,2-dihydrobenzo[*f*]chromen-3-one (14). Preparation by the general method for cyclization from 6-bromo-2-naphthol (3 mmol), 4-propylcinnamic acid (6 mmol), and

Amberlyst 15 ion-exchange resin (300 mg) in toluene. Yield: 24% (white solid); ^{1}H NMR ($CDCl_3$): δ = 8.03 (d, 1H, ar, J = 2.0 Hz), 7.78 (d, 1H, ar, J = 9.0 Hz), 7.69 (d, 1H, ar, J = 9.0 Hz), 7.55 (dd, 1H, ar, J = 9.0, 2.0 Hz), 7.37 (d, 1H, ar, J = 9.0 Hz), 7.08 (m, 2H, ar), 7.02 (m, 2H, ar), 4.90 (dd, 1H, C–H, J = 6.4, 2.6 Hz), 3.21 (dd, 1H, C–H, J = 15.8, 6.4 Hz), 3.18 (dd, 1H, C–H, J = 15.8, 2.6 Hz), 2.53 (t, 2H, CH_2, J = 7.4 Hz), 1.59 (s, 2H, CH_2, J = 7.4 Hz), 0.93 ppm (t, 3H, J = 7.4 Hz); ^{13}C NMR ($CDCl_3$): δ = 166.8 (C=O), 149.9 (ar, C–O), 142.2 (ar, C–C), 137.3 (ar, C–C), 132.1 (ar, C–C), 130.7 (ar, C–H), 130.6 (ar, C–H), 129.6 (ar, C–C), 129.3 (2C, ar, 2×C–H), 128.8 (ar, C–H), 126.6 (2C, ar, 2×C–H), 124.9 (ar, C–H), 119.2 (ar, C–C), 118.7 (ar, C–H), 118.2 (ar, C–C), 37.5 (CH_2), 37.3 (CH), 37.3 (CH_2), 24.3 (CH_2), 13.8 ppm (CH_3); IR (ATR): $\tilde{\nu}_{max}$ = 1761, 1502, 1225, 1191, 1138, 872, 814, 802 cm^{-1}; EIMS: (m/z): 396 [^{81}BrM]$^+$, 394 [^{79}BrM]$^+$; [M]$^+$ ($C_{22}H_{19}BrO_2$): 395.29.

1-(4-Ethylphenyl)-8-methyl-1,2-dihydrobenzo[*f*]chromen-3-one (15). Preparation by Pd-catalyzed introduction of a methyl group starting from the bromo-substituted splitomicin derivative **13** (0.50 mmol), trimethylaluminum (0.50 mmol), and tetrakis(triphenylphosphine)palladium (0.025 mmol). Reagents were held at reflux in 1,4-dioxane (3 mL, anhyd.) for 2 h. After cooling, the reaction mixture was diluted with H_2O. The product was extracted with CH_2Cl_2 and then purified by column chromatography on silica gel. Yield: 63% (white solid); ^{1}H NMR ($CDCl_3$): δ = 7.78 (d, 1H, ar, J = 8.3 Hz), 7.71 (d, 1H, ar, J = 8.6 Hz), 7.63 (s, 1H, ar), 7.32 (d and overlapping dd, 1H, ar, J = 9.0 Hz), 7.11–7.07 (m, 2H, ar), 7.04–7.00 (m, 2H, ar), 4.92 (dd, 1H, C–H, J = 2.4, 6.7 Hz), 3.22 (dd, 1H, C–H, J = 15.8, 6.7 Hz), 3.18 (dd, 1H, C–H, J = 15.8, 2.4 Hz), 2.58 (q, 2H, CH_2, J = 7.6 Hz), 2.38 (s, 3H, CH_3), 1.19 ppm (t, 3H, CH_3, J = 7.6 Hz); ^{13}C NMR ($CDCl_3$): δ = 167.4 (C=O), 149.1 (ar, C–O), 143.4 (ar, C–C), 137.8 (ar, C–C), 134.9 (ar, C–C), 131.3 (ar, C–C), 129.6 (ar, C–H), 129.1 (ar, C–H), 129.0 (ar, C–C), 128.0 (ar, 2×C–H), 127.7 (ar, C–H), 126.8 (ar, 2×C–H), 122.9 (ar, C–H), 117.7 (ar, C–C), 117.5 (ar, C–H), 37.5 (C–H), 37.2 (CH_2), 28.3 (CH_2), 21.3 (CH_3), 15.3 ppm (CH_3); IR (ATR): $\tilde{\nu}_{max}$ = 1765, 1511, 1208, 1141, 881, 820 cm^{-1}; EIMS: (m/z): 316;[37] [M]$^+$ ($C_{22}H_{20}O_2$): 316.39.

1-(4-Cyclopropylphenyl)-8-methyl-1,2-dihydrobenzo[*f*]chromen-3-one (16). A solution of the bromo-substituted splitomicin derivative 1-(4-bromophenyl)-8-methyl-1,2-dihydrobenzo[*f*]chromen-3-one (0.12 mmol), cyclopropylboronic acid (0.24 mmol), palladium acetate (12 μmol), tricyclohexyl phosphine (24 μmol), and 0.34 mmol potassium phosphate in a mixture of deoxygenated H_2O (0.1 mL) and toluene (1.5 mL) was placed in a sealed tube and stirred at 100 °C for 8 h. After cooling, the brown slurry was diluted with saturated NaCl (2 mL), and *tert*-butylmethylether (4 mL). The organic layer was then separated, dried over $MgSO_4$, and the solvents were removed under reduced pressure. The resulting residue was purified by column chromatography (cyclohexane/EtOAc, 9:1) yielding 34 mg (85%) of the desired product as an off-white solid; ^{1}H NMR ($CDCl_3$): δ = 9.38 (d, 1H, ar, J = 8.8 Hz), 7.89 (d, 1H, ar, J = 9.0 Hz), 7.56 (s, 1H, ar), 7.51 (dd, 1H, ar, J = 8.8, 2.0 Hz), 7.43–7.39 (m, 2H, ar), 7.17–7.14 (m, 2H, ar), 7.16 (d, 1H, ar, J = 9.0 Hz), 5.56 (dd, 1H, C–H, J = 13.8, 3.0 Hz), 3.24 (dd, 1H, C–H, J = 16.5, 13.8 Hz), 2.96 (dd, 1H, C–H, J = 16.5, 3.0 Hz), 2.52 (s, 3H, CH_3), 1.97–1.95 (m, 1H, *c*Pr-CH), 1.01–0.99 (m, 2H, *c*Pr-CH_2), 0.73–0.70 ppm (m, 2H, *c*Pr-CH_2); ^{13}C NMR ($CDCl_3$): δ = 193.2 (C=O), 163.2 (ar, C–O), 144.9 (ar, C–C), 137.0 (ar, C–H), 135.5 (ar, C–C), 134.4 (ar, C–C), 131.7 (ar, C–H), 129.5 (ar, C–C), 129.4 (ar, C–C), 127.6 (ar, C–H), 126.3 (ar, 2×C–H), 126.0 (ar, 2×C–H), 125.7 (ar, C–H), 118.8 (ar, C–H), 112.5 (ar, C–C), 79.5 (ar, CH), 45.6 (CH_2), 21.2 (CH_3), 15.2 (*c*Pr-CH), 9.4 (*c*Pr-CH_2), 9.4 ppm (*c*Pr-CH_2); IR (ATR): $\tilde{\nu}_{max}$ = 2901, 1670, 1595, 1237, 1221, 833, 815 cm^{-1}; EIMS: (m/z): 328;[37] [M]$^+$ ($C_{23}H_{20}O_2$): 328.41.

HPLC analysis of purity for compounds 13–16. HPLC was performed on a JASCO HPLC system under isocratic conditions. HPLC A refers to a Luna 5μ Phenylhexyl column (25 cm×4.6 mm, 5 μm; Phenomenex) and CH_3CN/H_2O mixtures (eluent A, in *v*/*v*). HPLC B refers to a Synergi Max-RP column (15 cm×4.6 mm, 4 μm; Phenomenex) and MeOH/H_2O mixtures (eluent B, in *v*/*v*). The concentrations of the compounds were ~100 μM, injection volumes were 30 μL, flow rate was 1 mL min^{-1}, and detection was performed with UV (λ = 254 nm).

Synthesis of thiobarbiturates. Compounds **25**–**29** were synthesized according to standard methods. Thiobarbituric acid (1.0 mmol) and the respective aldehyde (1.0 mmol) were a) condensed in HCl (10 mL, 2 M) at room temperature overnight (compounds **25**, **27**, and **28**), or b) dissolved in EtOH with HCl (three drops, 2 M) and heating (30 min, 70 °C) (compounds **26** and **29**). The resulting precipitate was filtered off. With method a), the precipitate was washed with hot H_2O. Compound **25** was recrystallized from MeOH. Compounds **27** and **28** were recrystallized from dioxane. With method b), the precipitate was washed with warm EtOH, hexanes and CH_3CN, and dried in vacuo. For compounds **27** and **28**, purity was determined by HPLC and UV detection using the following protocol: analytical column: Synergi 4μ Max-RP 80A (150×4.6 mm i.d.) packed with Synergi Max-RP (RP-12). Elution was performed at room temperature under gradient conditions. Eluent A was H_2O containing 0.05% TFA; eluent B was CH_3CN, also containing 0.05% TFA. Linear gradient conditions were as follows: 0–5 min, A = 100%; 5–15 min, linear increase to B = 100%; 15–45 min, B = 100%. A flow rate of 0.5 mL min^{-1} was maintained. UV detection at 254 nm was applied. For **26**: column was a Merck LiChrospher 60 RP-select B 5 μm, 250–4 mm; solvents: A: H_2O + 0.05% TFA, B: CH_3CN + 0.05% TFA; flow rate: 1 mL min^{-1}; λ = 210 nm. Gradient (*t* (min), solvent A, solvent B): 0.0, 90.0, 10.0; 4.0, 90.0, 10.0; 29.0, 0.0, 100.0; 31.0, 0.0, 100.0; 31.5, 90.0 10.0; 40.0, 90.0, 10.0. The purity of **29** was determined by ^{1}H NMR as it decomposed on the column. The thiobarbiturate inhibitors were all >95% pure.

5-(4-Phenylbenzylidene)-2-thiobarbituric acid (25). Yield: 59%; ^{1}H NMR ([D$_6$]DMSO): δ = 12.47 (s, 1H, NH), 12.37 (s, 1H, NH), 8.33 (s, 1H, C=CH), 8.31–8.29 (m, 2H, ar-H), 7.84–7.79 (m, 4H, ar-H), 7.54–7.42 ppm (m, 3H, ar-H); ^{13}C NMR ([D$_6$]DMSO): δ = 178.98 (C=S), 162.31 (C=O), 160.11 (C=O), 155.69 (O=C–C=C), 144.66 (Ar-C), 139.27 (Ar-C), 135.11 (Ar-CH), 132.16 (Ar-C), 129.71 (Ar-CH), 129.01 (Ar-CH), 127.51 (Ar-CH), 126.77 (Ar-CH), 119.18 ppm (1C, O=C–C=C); ESMS (direct mode): calcd/found (m/z): 308.0/308.1 [M]$^+$; anal. ($C_{13}H_{12}N_2O_3S$) calcd/found C: 66.22/65.93, H: 3.92/3.95, N: 9.08/9.01, S: 10.4/10.39.

5-(3-Indolydene)-2-thiobarbituric acid (26). Yield: 72%; ^{1}H NMR ([D$_6$]DMSO): δ = 12.95 (bs, 1H, ar-NH), 12.24 (s, 1H, NH), 12.19 (s, 1H, NH), 9.59 (d, 1H, ar-H, ^4J = 3.46), 8.73 (s, 1H, Ar-CH=C), 7.87–7.93 (m, 1H, ar-H), 7.58–7.64 (m, 1H, ar-H), 7.32–7.38 ppm (m, 2H, ar-H); ^{13}C NMR ([D$_6$]DMSO): δ = 178.12 (C=S), 163.23(C=O), 161.42 (C=O), 144.99 (C=C–H), 141.51 (Ar-C), 137.05 (Ar-C), 129.48 (O=C–C=C), 124.49 (Ar-CH), 123.55 (Ar-CH), 118.29 (Ar-CH), 113.81 (Ar-C), 112.83 (Ar-CH), 109.15 ppm (Ar-C); ESMS (direct mode, m/z): 271.0 [M]$^+$.

5-(3,4-Dimethoxybenzylidene)-2-thiobarbituric acid (27). Yield: 70%; ^{1}H NMR ([D$_6$]DMSO): δ = 12.39 (s, 1H, NH), 12.29 (s, 1H, NH), 8.43 (d, 1H, 2′-H, ^4J = 1.98 Hz), 8.28 (s, 1H, C=CH), 7.97 (dd, 1H, 6′-H, ^3J = 8.8 Hz, ^4J = 2.1 Hz), 7.14 (d, 1H, 5′-H, ^3J = 8.8 Hz), 3.90 (s, 3H, OCH_3), 3.82 ppm (s, 3H, OCH_3); ^{13}C NMR ([D$_6$]DMSO): δ = 178.74 (C=S), 162.81 (C=O), 160.60 (C=O), 156.93 (C=C–H), 154.72 (Ar-C), 148.35 (Ar-C), 132.91 (Ar-C), 126.05 (Ar-CH), 117.40 (Ar-CH), 115.77

(Ar-CH), 111.64 (C=O-C=C), 56.38 (OCH_3), 55.90 ppm (OCH_3); ESMS (direct mode, *m/z*): 292.0/291.9 $[M]^+$; t_R: 3.48 min.

5-(4-Methoxybenzylidene)-2-thiobarbituric acid (28). Yield: 49%; ^{1}H NMR ([D$_6$]DMSO): $\delta = 12.39$ (s, 1H, NH), 12.29 (s, 1H, NH), 8.43–8.41 (m, 2H, ar), 8.27 (s, 1H, C=CH), 7.09–7.07 (m, 2H, ar), 3.89 ppm (s, 3H, OCH_3); ^{13}C NMR ([D$_6$]DMSO): $\delta = 178.73$ (C=S), 164.52 (C=O), 162.80 (C=O), 160.60 (C–OCH_3), 156.43 (O=C–C=C), 138.54 (C-2′,6′), 125.80 (C-1′), 116.25 (O=C–C=C), 114.76 (C-3′,5′), 56.44 ppm (CH_3); ESMS (direct mode, *m/z*): 262.0/262.1. $[M]^+$; t_R: 3.52 min.

5-(4-Isopropylbenzylidene)-2-thiobarbituric acid (29). Yield: 63%; ^{1}H NMR ([D$_6$]DMSO): $\delta = 12.44$ (s, 1H, NH), 12.33 (s, 1H, NH), 8.28 (s, 1H, Ar-CH=C), 8.17 (d, 2H, ar-H, $^3J = 8.28$), 7.39 (d, 2H, ar-H, $^3J = 8.28$), 2.97 (sep, 1H, Ar-CH, $^3J = 6.91$), 1.23 (d, 6H, CH_3, $^3J = 6.90$) ppm; ^{13}C NMR ([D$_6$]DMSO): $\delta = 178.91$ (C=S), 162.32 (C=O), 160.02 (C=O), 156.28 (C=C–H), 154.97 (Ar-C), 134.86 (2C, Ar-CH), 130.71 (Ar-C), 126.75 (2C, Ar-CH), 118.42 (O=C–C=C), 34.11 (*CH*-$(CH_3)_2$), 23.81 (CH_3) ppm; ESMS (direct mode, *m/z*): 274.0 $[M]^+$.

Biochemical assays

Recombinant proteins. Human Sirt2 (N-terminally tagged with His_6) was expressed and purified as described previously[38] with minor modifications.[23] Sirt1 was expressed as a GST-tagged enzyme.[23] Identity and purity of the produced enzymes was verified using SDS electrophoresis. Deacetylase activity of the Sirt isoforms was dependent on NAD^+ and could be inhibited with nicotinamide.

Fluorescent deacetylase assay. All compounds were evaluated for their ability to inhibit recombinant sirtuins using a homogeneous fluorescent deacetylase assay.[29] Enzyme volumes depend on the activity of the preparation that is used and may vary from batch to batch. Usually, we adjust to 10–20% conversion of the substrate without inhibitor. Stock solutions of inhibitors were prepared in DMSO, and 3 μL or less of a suited DMSO inhibitor solution was added to the incubation mixture. The assay was carried out in 96-well plates. Briefly, a reaction volume of 60 μL contained the fluorescent histone deacetylase substrate ZMAL (10.5 μM), NAD^+ (500 μM), and Sirt1 or Sirt2. After incubation for 4 h at 37 °C, the deacetylation reaction was stopped. As stop solution we used trypsin buffer (60 μL) containing trypsin (6 mg mL^{-1}) from bovine pancreas (10000 BAEE units mg^{-1}) and the sirtuin inhibitor nicotinamide (4 mM). The microplate was incubated with this stop solution for 20 min at 37 °C. Fluorescence was then measured in a plate reader (BMG Polarstar) with a coumarin filter ($\lambda_{ex} = 390$ nm, $\lambda_{em} = 460$ nm). The amount of substrate remaining in the positive control with inhibitor versus negative control without inhibitor was employed to calculate inhibition. All determinations were carried out at least in duplicate. IC_{50} data were analyzed using GraphPad Prism software.

Computational details

All calculations were performed on a Pentium IV 2.2 GHz based Linux cluster (20 CPUs). The molecular structures of the inhibitors were generated using the MOE modeling package (Chemical Computing Group). The structures were energy minimized using the MMFF94s force field and the conjugate gradient method until the default derivative convergence criterion of 0.01 kcal (mol×Å)$^{-1}$ was met. The crystal structure of human Sirt2 (PDB code: 1J8F) was taken from the Protein Data Bank and prepared as described in previous docking studies.[22,23] Docking of the inhibitors was carried out with the program GOLD 3.2[28] and default settings (Cambridge Crystallographic Data Centre). Four co-crystallized water molecules, which can be observed in the nicotinamide binding pocket of the different Sirt2 monomers (A, B, and C), were included for ligand docking. GOLD offers the possibility to replace or use water molecules as mediators for a protein–ligand interaction (water toggle mode). The inclusion of these four water molecules was found in a former study to increase the quality of the docking results.[23] All torsion angles in each inhibitor were allowed to rotate freely. The binding site was defined on Ile169 with a radius of 15 Å. GoldScore was chosen as fitness function due to the success in our former docking studies. For each molecule, 10 docking runs were performed. The resulting solutions were clustered on the basis of the heavy atom RMSD values (1 Å). The top-ranked poses for each ligand were retained and analyzed graphically within MOE 2006.08 (Chemical Computing Group).[39]

GRID calculations. Interaction possibilities were analyzed using the GRID program (Molecular Discovery Inc.). GRID is an approach to predict noncovalent interactions between a molecule of known 3D structure (i.e. sirtuin) and a small group as a probe (representing chemical features of a ligand).[40] The calculations were performed using version 22 of the GRID program and the Sirt2 protein structure. The calculations were performed on a cube (20×20×20 Å, spacing 1 Å) including the nicotinamide binding pocket in order to search for binding sites complementary to the functional groups of the inhibitors. The following probes were used for calculation: carbonyl probe (O1) and hydrophobic methyl probe (C3). The calculated interaction fields were then viewed superimposed on the Sirt2 structure using the MOE program (figure 1 in the Supporting Information). The Conolly molecular surface of the binding pocket was calculated with the MOE program and colored according to molecular electrostatic potential (using MMF94 charges within MOE).

Virtual screening. We screened the Chembridge database for inhibitors structurally related to cambinol (**3**). The compounds of the Chembridge database were transformed into 3D molecular structures using the Omega module from OpenEye Software.[41] The ~328000 molecules were stored in a MOE database (Chemical Computing Group) and several physicochemical descriptors were calculated. The following filters for lead-like compounds were applied: a) M_r between 250 and 400, log$P < 5$, TPSA < 150 Å, at least one nitrogen atom. MACCS fingerprints were calculated for all compounds. Molecules similar to **3** (with an inverse distance > 0.7) were retrieved and further analyzed. The 390 compounds were docked into the Sirt2 protein structure as described above and using the GOLD program. GoldScores were calculated for all docking poses; 131 molecules were successfully docked into the nicotinamide binding pocket (showing a GoldScore between 30 and 62). The final selection of a small subset of compounds was based on visual inspection of the binding mode (only molecules showing a hydrogen bond to Gln167 were considered) and on the lipophilicity of the compounds (lower log*P* favored). Five thiobarbiturate and barbiturate derivatives were selected, which were found between rank 1 and 61).

AM1 calculations. The AM1 semi-empirical method was used to calculate the energetic differences between the tautomers of **7** and **8** (in vacuo, without considering the protein environment) to see which form is energetically more favorable. The energy differences were calculated because compounds **7** and **8** are stored as hydroxyquinoline tautomers in the Chembridge database, whereas it is known from the literature that the pyridone form is more likely.

MD simulations. Molecular dynamics and thermodynamic computations were carried out using AMBER 9.0[31] and the AMBER 1999SB force field.[42] We focused our MD simulations on inhibitors tested in our laboratory in the same biological in vitro assay. The initial structures of the Sirt2–inhibitor complexes were taken from the GOLD docking study. The ligand force field parameters were taken from the general AMBER force field (GAFF),[43] whereas AM1 ESP atomic partial charges were assigned to the inhibitors.[44] In the crystal structure of human Sirt2, each domain is associated with a divalent zinc ion coordinated to four anionic cysteine side groups. The divalent zinc ions were represented by the cationic dummy atom (CaDA) approach of Pang et al.,[25,45] which treats the zinc ion as tetrahedron-shaped divalent cation with dummy atoms filling the tetrahedral corners. Parameters and libraries for the tetrahedral zinc groups and anionic cysteine residues were obtained from Pang et al.[25,45] The Sirt2–inhibitor complexes were solvated in water boxes (TIP3) with the dimensions 18×18×18 Å. Periodic boundary conditions were applied, resulting in a final system with dimensions of approximately 90×90×90 Å. The distance between the outer boundary of the octahedral solvent box and the solute surface was set to 10 Å. Parameter/topology and coordinate files for the non-neutralized/non-solvated and the neutralized/solvated systems were prepared using the LEAP module in AMBER.

Eight sodium ions were added as counterions to neutralize the system. Prior to the free MD simulations, three steps of relaxation were carried out. In the first step, we kept the protein fixed with a constraint of 500 kcal mol^{-1} Å^{-1}, and we relaxed the position of the tetrahedron-shaped zinc cations (0.1 ps MD). In the second step, the zinc divalent cations and the inhibitor structures were relaxed for 0.5 ps, during which the protein atoms were restrained to the X-ray coordinates with a force constant of 500 kcal mol^{-1} Å^{-1}. In the final step, all restraints were removed, and the complexes were relaxed for 1 ps. The temperature of the relaxed system was then equilibrated at 300 K through 20 ps of MD using time steps of 2 fs. A constant volume periodic boundary was set to equilibrate the temperature of the system by the Langevin dynamics[32] using a collision frequency of 10 ps^{-1} and a velocity limit of five temperature units. During the temperature equilibration routine, the complex in the solvent box was restrained to the initial coordinates with a weak force constant of 10 kcal mol^{-1} Å^{-1}. The final coordinates of the temperature equilibration routine (after 20 ps) was then used to complete a 1-ns MD routine using 2-fs time steps, during which the temperature was kept at 300 K by the Langevin dynamics[32] using a collision frequency of 1 ps^{-1} and a velocity limit of 20 temperature units. The pressure of the solvated system was equilibrated at 1 bar at a certain density in a constant pressure periodic boundary by an isotropic pressure scaling method employing a pressure relaxation time of 2 ps. The time step of the free MD simulations was 2 fs with a cutoff of 9 Å for the nonbonded interaction, and SHAKE[42] was employed to keep all bonds involving hydrogen atoms rigid. Electrostatic interactions were computed using the Particle Mesh Ewald method.[33] The MD simulations of the Sirt2–inhibitor complexes were performed in total for 6 ns.

MM-PBSA. The net change in binding free energy accompanying the formation of the protein–ligand complex is approximated by Equation 1:

$$\Delta G = \Delta H - T\,\Delta S \quad (1)$$

in which T is the temperature of the system at 300 K. The binding free energy (ΔG) of the protein–ligand complex is computed as:

$$\Delta G = G_{\text{complex}} - [G_{\text{protein}} + G_{\text{ligand}}] \quad (2)$$

for which G_{complex} is the absolute free energy of the complex, G_{protein} is the absolute free energy of the protein, and G_{ligand} is the absolute free energy of the ligand. We extracted 100 snapshots (at time intervals of 2 ps) for each species (complex, protein, and ligand) from the last 200 ps of the MD simulations of the complexes. The enthalpy term in Equation 1 is dissected into sub-energy terms:

$$H_{\text{tot}} = H_{\text{gas}} + G_{\text{solv}} \quad (3)$$

$$H_{\text{gas}} = E_{\text{el}} + E_{\text{vdW}} + E_{\text{int}} \quad (4)$$

in which H_{gas} is the potential energy of the solute, which is determined as the sum of van der Waals (E_{vdw}), electrostatic (E_{el}) and internal energies (E_{int}) in the gas phase by using the SANDER module of AMBER.[31] G_{solv} is the solvation free energy for transferring the solute from vacuum into solvent and is a sum of electrostatic (G_{el}) and non-electrostatic (hydrophobic) contributions (G_{nonel}), as shown in Equation 5:

$$G_{\text{solv}} = G_{\text{el}} + G_{\text{nonel}} \quad (5)$$

G_{el} in Equation 5 was computed at a salt concentration of 0.15 M by the PBSA module of AMBER 9.0 by dividing implicitly solvated solute species into 0.4-Å cubic grid points and summing up the electrostatic potentials computed at each grid point. The electrostatic potential $\phi_{(r)}$ at a grid point r that is not at the solvent–solute boundary was computed by a linear Poisson–Boltzmann (PB) equation,[31] which is a 3D vector differential equation as in equation 6:

$$\nabla\varepsilon_{(r)}\,\nabla\phi_{(r)} = -4\pi\cdot\rho_{(r)} \quad (6)$$

in which $\varepsilon_{(r)}$ is the dielectric constant ($\varepsilon = 1$ for the solute interior, and $\varepsilon = 80$ for implicit PB water) and $\rho_{(r)}$ is the charge density. The grid point potentials were then summed up for each atom i to yield atomic potentials ϕ_i. The PB implicit solvent molecules at the solute–solvent boundary were allowed to energetically converge over 1000 iterations before the single-point Poisson computations were implemented by PBSA for each snapshot. A spherical solvent probe (radius) of 1.4 Å and atomic radii provided by the AMBER force field were used for the implicit solvent molecules and solute atoms, respectively, during the PBSA computations.

The absolute entropy was computed as an average over all snapshots by normal-mode analysis[46] integrated in the Nmode module of AMBER 9.0. An ensemble of different conformations was extracted from the MD trajectories, and each snapshot was analyzed by applying the MM-PBSA method.[47] The total entropy (S_{tot}), as formulated in Equation 7 arose from changes in the degree of freedom [translational (S_{trans}), rotational (S_{rot}), and vibrational (S_{vib})] of each species:[35]

$$S_{\text{tot}} = S_{\text{trans}} + S_{\text{rot}} + S_{\text{vib}} \quad (7)$$

Considering all absolute energy terms as given in Equation 2, the binding free energy ΔG takes the following form:

$$\Delta G_{\text{binding}} = [\Delta H_{\text{gas}} + \Delta G_{\text{solv}}] - T\,\Delta S_{\text{tot}} \quad (8)$$

Parameter/topology files used in MM-PBSA computations were prepared for the complex, the protein, and the inhibitors using the LEAP module. Snapshots extracted from trajectories were pre-minimized in the gas phase by the SANDER module by using a conjugate gradient method until the RMSD of the elements of the gradi-

ent vector was $< 10^{-4}$ kcal mol^{-1} Å^{-1}. Frequencies of the vibrational modes were computed at 300 K for these minimized structures including all snapshot atoms and using a harmonic approximation of the energies.[35]

Acknowledgements

Funding by the Deutsche Forschungsgemeinschaft (DFG) (Ju 295-4/1 and /2, Si 868/1-1) is gratefully acknowledged. We thank Ursula Predoiu and Alexander Rohe for technical assistance.

Keywords: binding free energy · drug design · hydrolases · sirtuin · virtual screening

[1] C. M. Grozinger, S. L. Schreiber, *Chem. Biol.* **2002**, *9*, 3–16.
[2] B. J. North, E. Verdin, *Adv. Genome Biol.* **2004**, *5*, 224.
[3] R. W. Johnstone, *Nat. Rev. Drug Discovery* **2002**, *1*, 287–299.
[4] S. Imai, C. M. Armstrong, M. Kaeberlein, L. Guarente, *Nature* **2000**, *403*, 795–800.
[5] S. Pagans, A. Pedal, B. J. North, K. Kaehlcke, B. L. Marshall, A. Dorr, C. Hetzer-Egger, P. Henklein, R. Frye, M. W. McBurney, H. Hruby, M. Jung, E. Verdin, M. Ott, *PLoS Biol.* **2005**, *3*, e41.
[6] H. Vaziri, S. K. Dessain, E. Ng Eaton, S. I. Imai, R. A. Frye, T. K. Pandita, L. Guarente, R. A. Weinberg, *Cell* **2001**, *107*, 149–159.
[7] O. R. Bereshchenko, W. Gu, R. Dalla-Favera, *Nat. Genet.* **2002**, *32*, 606–613.
[8] H. Ota, E. Tokunaga, K. Chang, M. Hikasa, K. Iijima, M. Eto, K. Kozaki, M. Akishita, Y. Ouchi, M. Kaneki, *Oncogene* **2006**, *25*, 176–185.
[9] T. F. Outeiro, E. Kontopoulos, S. Altman, I. Kufareva, K. E. Strathearn, A. M. Amore, C. B. Volk, M. M. Maxwell, J. C. Rochet, P. J. McLean, A. B. Young, R. Abagyan, M. B. Feany, B. T. Hyman, A. Kazantsev, *Science* **2007**, *317*, 516–519.
[10] S. Schäfer, M. Jung, *Arch. Pharm.* **2005**, *338*, 347–357.
[11] M. Biel, V. Wascholowski, A. Giannis, *Angew. Chem.* **2005**, *117*, 3248–3280; *Angew. Chem. Int. Ed.* **2007**, *46*, 5219–5222.
[12] C. M. Grozinger, E. D. Chao, H. E. Blackwell, D. Moazed, S. L. Schreiber, *J. Biol. Chem.* **2001**, *276*, 38837–38843.
[13] B. Heltweg, F. Dequiedt, E. Verdin, M. Jung, *Anal. Biochem.* **2003**, *319*, 42–48.
[14] A. Mai, S. Massa, S. Lavu, R. Pezzi, S. Simeoni, R. Ragno, F. R. Mariotti, F. Chiani, G. Camilloni, D. A. Sinclair, *J. Med. Chem.* **2005**, *48*, 7789–7795.
[15] A. J. Tervo, S. Kyrylenko, P. Niskanen, A. Salminen, J. Leppanen, T. H. Nyronen, T. Jarvinen, A. Poso, *J. Med. Chem.* **2004**, *47*, 6292–6298.
[16] A. J. Tervo, T. Suuronen, S. Kyrylenko, E. Kuusisto, P. H. Kiviranta, A. Salminen, J. Leppanen, A. Poso, *J. Med. Chem.* **2006**, *49*, 7239–7241.
[17] C. Gey, S. Kyrylenko, L. Hennig, L. H. Nguyen, A. Buttner, H. D. Pham, A. Giannis, *Angew. Chem.* **2007**, *119*, 5311–5314; *Angew. Chem. Int. Ed. Engl.* **2007**, *46*, 5219–5222.
[18] B. Heltweg, T. Gatbonton, A. D. Schuler, J. Posakony, H. Li, S. Goehle, R. Kollipara, R. A. Depinho, Y. Gu, J. A. Simon, A. Bedalov, *Cancer Res.* **2006**, *66*, 4368–4377.
[19] A. D. Napper, J. Hixon, T. McDonagh, K. Keavey, J. F. Pons, J. Barker, W. T. Yau, P. Amouzegh, A. Flegg, E. Hamelin, R. J. Thomas, M. Kates, S. Jones, M. A. Navia, J. O. Saunders, P. S. DiStefano, R. Curtis, *J. Med. Chem.* **2005**, *48*, 8045–8054.
[20] J. Trapp, R. Meier, D. Hongwiset, M. U. Kassack, W. Sippl, M. Jung, *ChemMedChem* **2007**, *2*, 1419–1431.
[21] K. T. Howitz, K. J. Bitterman, H. Y. Cohen, D. W. Lamming, S. Lavu, J. G. Wood, R. E. Zipkin, P. Chung, A. Kisielewski, L. L. Zhang, B. Scherer, D. A. Sinclair, *Nature* **2003**, *425*, 191–196.
[22] J. Trapp, A. Jochum, R. Meier, L. Saunders, B. Marshall, C. Kunick, E. Verdin, P. G. Goekjian, W. Sippl, M. Jung, *J. Med. Chem.* **2006**, *49*, 7307–7316.
[23] R. C. Neugebauer, U. Uchiechowska, R. Meier, H. Hruby, V. Valkov, E. Verdin, W. Sippl, M. Jung, *J. Med. Chem.* **2008**, *51*, 1203–1213.
[24] J. Posakony, M. Hirao, S. Stevens, J. A. Simon, A. Bedalov, *J. Med. Chem.* **2004**, *47*, 2635–2644.
[25] Y. P. Pang, *J. Mol. Model.* **1999**, *5*, 196–202.
[26] J. L. Avalos, K. M. Bever, C. Wolberger, *Mol. Cell* **2005**, *17*, 855–868.
[27] M. S. Finnin, J. R. Donigian, N. P. Pavletich, *Nat. Struct. Biol.* **2001**, *8*, 621–625.
[28] G. Jones, P. Willet, R. C. Glen, A. R. Leach, R. Taylor, *J. Mol. Biol.* **1997**, *267*, 727–748.
[29] B. Heltweg, J. Trapp, M. Jung, *Methods* **2005**, *36*, 332–337.
[30] J. R. Tame, *J. Comput. Aided Mol. Des.* **2005**, *19*, 445–451.
[31] D. A. Case, T. E. I. Cheatham, T. Darden, H. Gohlke, R. Luo, K. M. J. Merz, A. Onufriev, C. Simmerling, W. Wang, R. Woods, *J. Comput. Chem.* **2005**, *26*, 1668–1688.
[32] R. W. Pastor, B. R. Brooks, A. Szabo, *Mol. Phys.* **1988**, *65*, 1409–1419.
[33] T. Darden, D. York, L. Pedersen, *J. Chem. Phys.* **1993**, *98*, 10089–10092.
[34] J. P. Ryckaert, G. Ciccotti, H. J. C. Berendsen, *J. Comput. Phys.* **1977**, *23*, 327–341.
[35] H. Gohlke, D. A. Case, *J. Comput. Chem.* **2004**, *25*, 238–250.
[36] K. S. Shindler, E. Ventura, T. S. Rex, P. Elliott, A. Rostami, *Invest. Ophthalmol. Vis. Sci.* **2007**, *48*, 3602–3609.
[37] R. U. Kadam, J. Tavares, V. M. Kiran, A. Cordeiro, A. Ouaissi, N. Roy, *Chem. Biol. Drug Des.* **2008**, *71*, 501–506.
[38] B. J. North, B. Schwer, N. Ahuja, B. Marshall, E. Verdin, *Methods* **2005**, *36*, 338–345.
[39] Chemical Computing Group Inc., Montreal, QC (Canada), **2006**.
[40] P. J. Goodford, *J. Med. Chem.* **1985**, *28*, 849–857.
[41] OpenEye Scientific Software, Santa Fe, NM (USA), **2007**.
[42] V. Hornak, R. Abel, A. Okur, B. Strockbine, A. Roitberg, C. Simmerling, *Proteins* **2006**, *65*, 712–725.
[43] J. Wang, R. M. Wolf, J. W. Caldwell, P. A. Kollman, D. A. Case, *J. Comput. Chem.* **2004**, *25*, 1157–1174.
[44] J. Wang, W. Wang, P. A. Kollman, D. A. Case, *J. Mol. Graphics Modell.* **2006**, *25*, 247–260.
[45] Y. P. Pang, K. Xu, J. E. Yazal, F. G. Prendergas, *Protein Sci.* **2000**, *9*, 1857–1865.
[46] D. A. Case in *Rigidity Theory and Applications* (Ed.: M. F. Thorpe), Plenum, **1999**, pp. 329–344.
[47] W. Wang, P. A. Kollman, *J. Mol. Biol.* **2000**, *303*, 567–582.

Received: April 1, 2008
Revised: September 9, 2008
Published online on November 4, 2008

